www.ietdl.org

Published in IET Communications
Received on 12th April 2013
Revised on 18th October 2013
Accepted on 19th December 2013
doi: 10.1049/iet-com.2013.0310

ISSN 1751-8628

Performance analysis of asynchronous optical code division multiple access with spectral-amplitude-coding

Mohammad Ali Sedaghat[1], *Ralf R. Müller*[2], *Farokh Marvasti*[3]

[1]*Department of Electronics and Telecommunications, Norwegian University of Science and Technology (NTNU), Trondheim, Norway*
[2]*Department of Electrical, Electronic and Communication Engineering, Friedrich-Alexander University Erlangen-Nuremberg, Germany*
[3]*Department of Electrical Engineering, Sharif University of Technology, Tehran, Iran*
E-mail: mohammad.sedaghat@iet.ntnu.no

Abstract: In this study, the performance of a spectral-amplitude-coding optical code division multiple access (SAC-OCDMA) system in the asynchronous regime is evaluated using a Gaussian approximation of the decision variable for codes with fixed cross-correlation used in SAC-OCDMA systems. The authors consider the effect of phase-induced intensity noise (PIIN), thermal noise and shot noise. Moreover, the validity of the Gaussian approximation is confirmed by a Kolmogorov–Smirnov fitness test. For sake of comparison, the bit error rate (BER) of the asynchronous SAC-OCDMA system is also plotted numerically in comparison with the BER of the synchronous SAC-OCDMA. They show that a SAC-OCDMA system without any time management for the users, that is, the asynchronous regime, has a better performance than the synchronous SAC-OCDMA when PIIN effect exists.

1 Introduction

Optical code division multiple access (OCDMA) systems are among attractive candidates for access networks in optical communications. In these systems, each user is assigned a unique spreading sequence (signature) to be distinguished from the other users. A major advantage of OCDMA systems compared with other multiple access techniques is that they do not require traffic management and system synchronisation. Among OCDMA systems, spectral-amplitude-coding OCDMA (SAC-OCDMA) attracts more attention than before because of low complexity devices [1] and the ability in suppressing the mean of multiple-access interference (MAI) [2]. The main performance degrading factor in SAC-OCDMA systems is the phase-induced intensity noise (PIIN) which originates from the incoherency of the broadband light sources of different transmitters [3].

Several signature codesets with fixed weight and fixed cross-correlation between codes have been proposed for the SAC-OCDMA systems, such as m-sequences [4], Hadamard [5], modified-quadratic congruence (MQC) codes [6], modified frequency-hopping codes [7], balanced incomplete block design codes [8] and modified double weight codes [9]. To alleviate the PIIN in the SAC-OCDMA systems, the codes with the minimum cross-correlation between codes are used.

Recently, Noshad and Jamshidi [10] presented both lower and upper bounds of the bit error rate (BER) for the synchronous SAC-OCDMA system which uses a family of codes with fixed weight and fixed cross-correlation. Shalaby [11] has obtained the BER of the synchronous SAC-OCDMA system based on Gaussian approximation of MAI for codes with fixed cross-correlation. However, there is no performance evaluation for the asynchronous SAC-OCDMA system which is a more attractive candidate in the implementation. In this paper, we obtain the BER of the asynchronous SAC-OCDMA system. In the analysis, PIIN, shot noise and thermal noise are considered. It is shown that the effect of PIIN is less severe in the asynchronous regime than in the synchronous regime. Therefore, the performance is outperformed if there is no time management in SAC-OCDMA.

The rest of the paper is organised as follows. Section 2 describes the SAC-OCDMA system model. The BER is evaluated in Section 3. Section 4 shows the numerical results and finally Section 5 concludes the paper.

2 SAC-OCDMA system model

In a SAC-OCDMA system, each user is assigned a code sequence of length L, weight w and cross-correlation λ from a code set $C(L, w, \lambda)$. The intensities of the spectral components for each pulse are modulated using these codes [1]. A SAC-OCDMA system with N users is considered. The optical frequency and bandwidth are denoted by f_c and

$\Delta\nu$, respectively. In the analysis, the first user is considered to be the desired user. A balanced detection scheme is utilised in the receiver [1] which consists of a coupler and two branches. The upper branch uses an amplitude mask of $c_1 \in C$ and a photodetector while the lower branch uses the photodetector and an amplitude mask of $\bar{c}_1$ [12]. To mitigate the mean of MAI, it is necessary to have an optical coupler with ratio 1: $\lambda/(w-\lambda)$ [12]. The outputs of the photodetectors are subtracted and compared with a threshold to detect the information bit of the desired user [2]. Since it is assumed that the photodetectors are identical, the output of the subtractor can be written as

$$s = \frac{\mathcal{R}}{T_b}\left[\int_0^{T_b} |E_U(t)|^2 dt - \int_0^{T_b} |E_L(t)|^2 dt\right] \quad (1)$$

where $\mathcal{R}$ denotes the responsivity of the photodetectors, T_b is the bit time duration. Also $E_U(t)$ and $E_L(t)$ denote the incident field of the upper branch and the lower branch, respectively. We consider a SAC-OCDMA system with asynchronous users where $g(t)$ is the normalised light field envelop of users in the spectral width $\Delta\nu/L$ and P is the power of the users. Then, in a bit time duration of the first user $E_U(t)$ and $E_L(t)$ can be shown as (see (2 and 3))

where $\Delta w = 2\pi\ \Delta\nu/L$, $w_0 = 2\pi\ (f_c - \Delta\nu/2 - \Delta\nu/L)$, $\phi_{ni}(t)$ and $\phi'_{ni}(t)$ are the phases of the optical signals with zero initial condition in the ith chip of the first bit and of the second bit, respectively, for the nth user. In (2) and (3), θ_{ni} and θ'_{ni} are the initial phases of light for first and the second bits of the nth user, respectively. d_{n1} and d_{n2} are the first and the second information bits of the nth user, respectively. Furthermore, τ_n and $\tau'_n = \tau_n - T_b$ are the relative delays of the first and the second bits of the nth user to the time reference of the first user, respectively. It is important to note that we assume $\tau_1 = 0$ and τ_n is a uniform random variable in [0, T_b] for $n \neq 1$. Moreover, $\phi_{ni}(t)$ is modelled as a Wiener–Levy process as explained in [13] and θ_{ni} and θ'_{ni} are the uniform random variables in [0, 2π]. It is important to note that because of the incoherent sources being used, all phases of optical fields in all of the spectral bins for all users are supposed to be independent [10].

3 BER analysis

In this section, we try to find the BER of the system described in Section 2. The main assumption in our analysis is that because of the large number of users and based on the central limit theorem (CLT), s [in (1)] can be considered as a Gaussian random variable. In the numerical results section, validity of the Gaussian approximation is investigated by comparing simulation results and analytical results. Base on the Gaussian approximation, it is enough to find mean and variance of s. The probability of error conditioned on the MAI is obtained and then the total probability of error is calculated by taking the average over all possible MAIs. In the following subsections, we derive the means and the variances of the outputs of upper and lower branches.

3.1 Upper branch

The output of the photodetector in the upper branch can be written as

$$I_U = \frac{\mathcal{R}}{T_b}\int_0^{T_b} |E_U(t)|^2 dt = I_{1U} + I_{2U} \quad (4)$$

where I_{1U} and I_{2U} are given as follows

$$I_{1U} = \frac{P\mathcal{R}}{T_b L}\int_0^{T_b} \sum_i \sum_n \left(d_{n1} g(t-\tau_n)^2 + d_{n2} g(t-\tau'_n)^2\right) c_n(i) c_1(i) dt$$
$$= \frac{P\mathcal{R}}{L}\left(d_{11} w + \sum_{n>1} \frac{\lambda}{T_b}\int_0^{T_b} \left(d_{n1} g(t-\tau_n)^2 + d_{n2} g(t-\tau'_n)^2\right) dt\right) \quad (5)$$

(see (6) at the bottom of the next page)

It is important to note that the desired bit of the first user is supposed to be d_{11}. Owing to the random initial phases, I_{1U} and I_{2U} are uncorrelated. Therefore it is enough to obtain the mean and the variance of each term individually. The mean of I_{1U} is obtained as

$$E(I_{1U}) = \frac{\mathcal{R}P}{L}\left(d_{11} w + \frac{\lambda}{T_b^2}\int_0^{T_b}\int_0^{T_b} g(t-\tau)^2 d\tau dt \sum_{n>1}(d_{n1} + d_{n2})\right)$$
$$= \frac{\mathcal{R}P}{L}\left(d_{11} w + \lambda(\kappa_1 + \kappa_2)\frac{1}{T_b^2}\int_0^{T_b}\int_0^{T_b} g(t-\tau)^2 d\tau dt\right) \quad (7)$$

where

$$\kappa_1 = \sum_{n>1} d_{n1},\ \ \kappa_2 = \sum_{n>1} d_{n2} \quad (8)$$

Owing to the random initial phases, that is, θ_{ni}'s and θ'_{ni}'s, the mean of I_{2U} is equal to zero. Moreover, calculation of $\sigma^2_{I_{1U}}$ is not required because it will be seen in the next subsection that

$$E_U(t) = \sqrt{\frac{P}{L}}\sum_n \sum_i \left[d_{n1} g(t-\tau_n) e^{j\left(w_0(t-\tau_n) + i\Delta w(t-\tau_n) + \phi_{ni}(t-\tau_n) + \theta_{ni}\right)}\right.$$
$$\left. + d_{n2} g(t-\tau'_n) e^{j\left(w_0(t-\tau'_n) + i\Delta w(t-\tau'_n) + \phi'_{ni}(t-\tau'_n) + \theta'_{ni}\right)}\right] c_n(i) c_1(i) \quad (2)$$

$$E_L(t) = \sqrt{\frac{\lambda}{w-\lambda}\frac{P}{L}}\sum_n \sum_i \left[d_{n1} g(t-\tau_n) e^{j\left(w_0(t-\tau_n) + i\Delta w(t-\tau_n) + \phi_{ni}(t-\tau_n) + \theta_{ni}\right)}\right.$$
$$\left. + d_{n2} g(t-\tau'_n) e^{j\left(w_0(t-\tau'_n) + i\Delta w(t-\tau'_n) + \phi'_{ni}(t-\tau'_n) + \theta'_{ni}\right)}\right] c_n(i) \bar{c}_1(i) \quad (3)$$

the term

$$\frac{P\mathcal{R}}{L}\left(\sum_{n>1}\frac{\lambda}{T_\mathrm{b}}\int_0^{T_\mathrm{b}}\left(d_{n1}g(t-\tau_n)^2+d_{n2}g(t-\tau_n')^2\right)\mathrm{d}t\right) \quad (9)$$

appears in the lower branch, hence this term is mitigated in s. Therefore we only obtain the variance of $I_{2\mathrm{U}}$. Owing to $T_\mathrm{b}\gg(L/\Delta v)$, for $m=n$ and $i\neq j$ the summation in (6) vanishes [11]. Therefore $I_{2\mathrm{U}}$ can be written as (see (10))

It can be proven that α_1, α_2, α_3 and α_4, which are defined in (10), are uncorrelated. Therefore we have

$$\sigma^2_{I_{2\mathrm{U}}}=\sigma^2_{\alpha_1}+\sigma^2_{\alpha_2}+\sigma^2_{\alpha_3}+\sigma^2_{\alpha_4} \quad (11)$$

The variance of α_1 is calculated as

$$\begin{aligned}\sigma^2_{\alpha_1}=&2\left(\frac{P\mathcal{R}}{T_\mathrm{b}L}\right)^2\sum_{m>n}\sum_{i,j}\sum_{m'>n'}\sum_{i',j'}c_n(i)c_m(j)c_1(i)c_1(j)\\&c_{n'}(i')c_{m'}(j')c_1(i')c_1(j')E_\tau E_\phi\\&\iint\Big\{d_{n1}d_{m1}d_{n'1}d_{m'1}g(t-\tau_n)g(t-\tau_m)g(s-\tau_{n'})g(s-\tau_{m'})\\&\times\cos\Big[w_0(\tau_m-\tau_n-\tau_{m'}+\tau_{n'})+\Delta w((i-j)t\\&-(i'-j')s+j\tau_m-i\tau_n-j'\tau_{m'}+i'\tau_{n'})\\&+\phi_{ni}(t-\tau_n)-\phi_{mj}(t-\tau_m)-\phi_{n'i'}(s-\tau_{n'})\\&+\phi_{m'j'}(s-\tau_{m'})+\theta_{ni}-\theta_{mj}-\theta_{n'i'}+\theta_{m'j'}\Big]\Big\}\,\mathrm{d}t\,\mathrm{d}s\end{aligned} \quad (12)$$

The expectation in (12) is not zero if

$$\theta_{ni}-\theta_{mj}-\theta_{n'i'}+\theta_{m'j'}=0 \quad (13)$$

The condition given in (13) is satisfied if

$$i=i',\ j=j',\ n=n',\ m=m' \quad (14)$$

Therefore the variance of α_1 can be calculated as

$$\begin{aligned}\sigma^2_{\alpha_1}=&2\left(\frac{P\mathcal{R}}{T_\mathrm{b}L}\right)^2\sum_{m>n}\sum_{i,j}c_n(i)c_m(j)c_1(i)c_1(j)E_\tau E_\phi\\&\iint d_{n1}d_{m1}g(t-\tau_n)g(t-\tau_m)g(s-\tau_n)g(s-\tau_m)\\&\times\cos\Big[\Delta w((i-j)t-(i-j)s)+\phi_{ni}(t-\tau_n)\\&-\phi_{mj}(t-\tau_m)-\phi_{ni}(s-\tau_n)+\phi_{mj}(s-\tau_m)\Big]\mathrm{d}t\,\mathrm{d}s\end{aligned} \quad (15)$$

To calculate (15), the following property of Gaussian random variables is used: for a Gaussian random variable χ and constant χ_0 we can write [13]

$$E(\cos(\chi_0+\chi))=\cos(\chi_0)\mathrm{e}^{-\left(\sigma^2_\chi/2\right)} \quad (16)$$

where σ^2_χ is the variance of χ. Moreover, for the Wiener–Levy process $\phi_{ni}(t)$, it has been shown that [14]

$$E\left\{\left[\phi_{ni}(t_a)-\phi_{ni}(t_b)\right]^2\right\}=\underline{\mathrm{def}}D_{\phi_{ni}}(t_a,t_b)=2\frac{|t_a-t_b|}{\tau_\mathrm{c}} \quad (17)$$

where τ_c is the coherence time of the sources. It is assumed that all sources have the same coherence time. By using (16) and (17), $\sigma^2_{\alpha_1}$ can be calculated as (see (18) at the bottom of next page)

where

$$R^n_g(t,s)\underline{\mathrm{def}}\begin{cases}\dfrac{1}{T_\mathrm{b}}\displaystyle\int_0^{T_\mathrm{b}}g(t-\tau)g(s-\tau)\,\mathrm{d}\tau & n\neq 1\\ g(t)g(s) & n=1\end{cases} \quad (19)$$

Exact calculation of (18) is too complex. However, it can be

$$\begin{aligned}I_{2\mathrm{U}}=&\frac{2\mathcal{R}P}{T_\mathrm{b}L}\int_0^{T_\mathrm{b}}\sum_{m\geq n,(n,i)\neq(m,j)}c_n(i)c_m(j)c_1(i)c_1(j)\times\Big\{d_{n1}d_{m1}g(t-\tau_n)g(t-\tau_m)\cos\left(w_0(\tau_m-\tau_n)+\Delta w((i-j)t+j\tau_m-i\tau_n)\right.\\&\times\ d_{n1}d_{m2}g(t-\tau_m')g(t-\tau_n)\cos\Big(w_0(\tau_m'-\tau_n)+\Delta w((i-j)t+j\tau_m'-i\tau_n)+\phi_{ni}(t-\tau_n)-\phi_{mj}'(t-\tau_m')+\theta_{ni}-\theta_{mj}'\Big)\\&+\ d_{n2}d_{m1}g(t-\tau_n')g(t-\tau_m)\cos\Big(w_0(\tau_m-\tau_n')+\Delta w((i-j)t+j\tau_m-i\tau_n')+\phi_{ni}'(t-\tau_n')-\phi_{mj}(t-\tau_m)+\theta_{ni}'-\theta_{mj}\Big)\\&+d_{n2}d_{m2}g(t-\tau_m')g(t-\tau_n')\cos+\Big(w_0(\tau_m'-\tau_n')+\Delta w((i-j)t+j\tau_m'-i\tau_n')+\phi_{ni}'(t-\tau_n')-\phi_{mj}'(t-\tau_m')+\theta_{ni}'-\theta_{mj}'\Big)\Big\}\mathrm{d}t\end{aligned} \quad (6)$$

$$\begin{aligned}I_{2\mathrm{U}}=&\frac{2\mathcal{R}P}{T_\mathrm{b}L}\int_0^{T_\mathrm{b}}\sum_{m>n,i,j}c_n(i)c_m(j)c_1(i)c_1(j)\times\Big\{d_{n1}d_{m1}g(t-\tau_n)g(t-\tau_m)\cos(w_0(\tau_m-\tau_n)+\Delta w((i-j)t+j\tau_m-i\tau_n)\\&+\phi_{ni}(t-\tau_n)-\phi_{mj}(t-\tau_m)+\theta_{ni}-\theta_{mj})+d_{n1}d_{m2}g(t-\tau_m')g(t-\tau_n)\cos\left(w_0(\tau_m'-\tau_n)+\Delta w((i-j)t+j\tau_m'-i\tau_n)\right.\\&+\phi_{ni}(t-\tau_n)-\phi_{mj}'(t-\tau_m')+\theta_{ni}-\theta_{mj}')+d_{n2}d_{m1}g(t-\tau_n')g(t-\tau_m)\cos(w_0(\tau_m-\tau_n')\\&+\Delta w((i-j)t+j\tau_m-i\tau_n')+\phi_{ni}'(t-\tau_n')-\phi_{mj}(t-\tau_m)+\theta_{ni}'-\theta_{mj})+d_{n2}d_{m2}g(t-\tau_m')g(t-\tau_n')\\&+\cos(w_0(\tau_m'-\tau_n')+\Delta w((i-j)t+j\tau_m'-i\tau_n')+\phi_{ni}'(t-\tau_n')-\phi_{mj}'(t-\tau_m')+\theta_{ni}'-\theta_{mj}')\Big\}\mathrm{d}t\underline{\mathrm{def}}\alpha_1+\alpha_2+\alpha_3+\alpha_4\end{aligned} \quad (10)$$

doi: 10.1049/iet-com.2013.0310

shown that for $i \neq j$ the summation in (18) vanishes if $T_b \gg L/\Delta v$. Therefore (18) can be written as

$$\begin{aligned}\sigma_{\alpha_1}^2 &= 2\left(\frac{P\mathcal{R}}{T_b L}\right)^2 \sum_{m>n}\sum_i c_n(i)c_m(i)c_1(i)d_{n1}d_{m1} \\ &\quad \times \int\int R_g^n(t,s)R_g^m(t,s)e^{-2(|t-s|/\tau_c)}\,dt\,ds \\ &= 2h\left(\frac{P\mathcal{R}}{T_b L}\right)^2 \sum_{m>1}\sum_i c_m(i)c_1(i)d_{11}d_{m1} \\ &\quad + 2h'\left(\frac{P\mathcal{R}}{T_b L}\right)^2 \sum_{m>n>1}\sum_i c_n(i)c_m(i)c_1(i)d_{n1}d_{m1} \end{aligned} \quad (20)$$

where

$$\begin{aligned} h &= g(t)g(s)R_g^m(t,s)e^{-2(|t-s|/\tau_c)}\,dt\,ds \\ h' &= R_g^m(t,s)^2 e^{-2(|t-s|/\tau_c)}\,dt\,ds \end{aligned} \quad (21)$$

Finally, $\sigma_{\alpha_1}^2$ can be written as

$$\begin{aligned}\sigma_{\alpha_1}^2 &= 2h\left(\frac{P\mathcal{R}}{T_b L}\right)^2 \lambda d_{11}\sum_{m>1} d_{m1} \\ &\quad + 2h'\left(\frac{P\mathcal{R}}{T_b L}\right)^2 \lambda\frac{w}{L}\sum_{m>n>1} d_{n1}d_{m1} \end{aligned} \quad (22)$$

By the same method as in calculating $\sigma_{\alpha_1}^2$, we obtain

$$\begin{aligned}\sigma_{\alpha_2}^2 &= 2h\left(\frac{P\mathcal{R}}{T_b L}\right)^2 \lambda d_{11}\sum_{m>1} d_{m2} \\ &\quad + 2h'\left(\frac{P\mathcal{R}}{T_b L}\right)^2 \lambda\frac{w}{L}\sum_{m>n>1} d_{n1}d_{m2} \end{aligned} \quad (23)$$

$$\sigma_{\alpha_3}^2 = 2h'\left(\frac{P\mathcal{R}}{T_b L}\right)^2 \lambda\frac{w}{L}\sum_{m>n>1} d_{n2}d_{m1} \quad (24)$$

$$\sigma_{\alpha_4}^2 = 2h'\left(\frac{P\mathcal{R}}{T_b L}\right)^2 \lambda\frac{w}{L}\sum_{m>n>1} d_{n2}d_{m2} \quad (25)$$

From (23)–(25), $\sigma_{I_{2U}}^2$ can be written as

$$\sigma_{I_{2U}}^2 = 2h\left(\frac{P\mathcal{R}}{T_b L}\right)^2 \lambda d_{11}(\kappa_1+\kappa_2) + 2h'\left(\frac{P\mathcal{R}}{T_b L}\right)^2 \lambda\frac{w}{L}\kappa_3 \quad (26)$$

where κ_1 and κ_2 are defined in (8) and

$$\kappa_3 = \sum_{m>n>1} d_{n1}d_{m1} + d_{n1}d_{m2} + d_{n2}d_{m1} + d_{n2}d_{m2} \quad (27)$$

κ_3 can be calculated as

$$\kappa_3 = \frac{1}{2}(\kappa_1+\kappa_2)^2 - \frac{1}{2}(\kappa_1+\kappa_2) - \kappa_4 \quad (28)$$

where $\kappa_4 = \sum_{n>1} d_{n1}d_{n2}$. As it will be seen in the numerical result section, using (28) makes our calculation simple.

3.2 Lower branch

The output of the photodetector in the lower branch can be written as

$$I_L = \frac{\mathcal{R}}{T_b}\int_0^{T_b} |E_L(t)|^2 dt = I_{1L} + I_{2L} \quad (29)$$

where $I_{1\,L}$ and $I_{2\,L}$ are defined as follows

$$\begin{aligned} I_{1L} &= \frac{\lambda}{w-\lambda}\frac{P\mathcal{R}}{T_b L}\int_0^{T_b} \sum_i\sum_n \left(d_{n1}g(t-\tau_n)^2 + d_{n2}g(t-\tau_n')^2\right) \\ &\quad \times c_n(i)\bar{c}_1(i)\,dt \\ &= \frac{P\mathcal{R}\lambda}{LT_b}\left(\sum_{n>1}\int_0^{T_b} \left(d_{n1}g(t-\tau_n)^2 + d_{n2}g(t-\tau_n')^2\right)dt\right) \end{aligned} \quad (30)$$

(see (31) at the bottom of next page)

From (1), (5) and (30), it can be easily observed that $I_{1\,L}$ is mitigated by the second term of I_{1U}. Therefore the calculation of the mean and the variance of $I_{2\,L}$ is enough. The mean and the variance of $I_{2\,L}$ can be easily obtained by using the similar steps as in (11)–(26) as

$$E(I_{2L}) = 0 \quad (32)$$

$$\sigma_{I_{2L}}^2 = 2h'\left(\frac{\lambda}{w-\lambda}\right)^2\left(\frac{P\mathcal{R}}{T_b L}\right)^2 \lambda\left(1-\frac{w}{L}\right)\kappa_3 \quad (33)$$

3.3 Statistics of decision variable

The decision variable is approximated by a Gaussian random variable as

$$s \sim \mathcal{N}\left(\frac{\mathcal{R}P}{L}d_{11}w,\ \sigma_s^2(d_{11},\ \kappa_1,\ \kappa_2,\ \kappa_4)\right) \quad (34)$$

$$\begin{aligned}\sigma_{\alpha_1}^2 &= 2\left(\frac{P\mathcal{R}}{T_b L}\right)^2 \sum_{m>n}\sum_{i,j} c_n(i)c_m(j)c_1(i)c_1(j)E_\tau \times d_{n1}d_{m1}g(t-\tau_n)g(t-\tau_m)g(s-\tau_n) \\ &\quad g(s-\tau_m)\cos\left[\Delta w(i-j)(t-s)\right]e^{-2(|t-s|/\tau_c)}\,dt\,ds \\ &= 2\left(\frac{P\mathcal{R}}{T_b L}\right)^2 \sum_{m>n}\sum_{i,j} c_n(i)c_m(j)c_1(i)c_1(j) \times d_{n1}d_{m1}R_g^n(t,s)R_g^m(t,s)\cos\left(\Delta w(i-j)(t-s)\right)e^{-2(|t-s|/\tau_c)}\,dt\,ds \end{aligned} \quad (18)$$

where

$$\sigma_s^2(d_{11}, \kappa_1, \kappa_2, \kappa_4) = \sigma_{I_{2U}}^2 + \sigma_{I_{2L}}^2 + \sigma_T^2 + \sigma_S^2 \quad (35)$$

Let σ_T^2 and σ_S^2 represent the variances of thermal and shot noises, respectively which are calculated as [11]

$$\sigma_T^2 = 4k_B T^\circ B_e / R_L \quad (36)$$

$$\sigma_S^2 = 2eB_e(E(I_U) + E(I_L)) \quad (37)$$

where $k_B = 1.38 \times 10^{-23}$ J/K is the Boltzmann's constant, T° is the receiver noise temperature, R_L is the receiver load resistance, $e = 1.6 \times 10^{-19}$ C is the electron charge and B_e is the receiver electrical bandwidth, that is, $B_e = 1/2T_b$.

Finally, the total probability of error can be expressed as

$$P_e = \frac{1}{2} \sum_{\kappa_1,\kappa_2,\kappa_4} P(\kappa_1, \kappa_2, \kappa_4) \times \left[P(e|d_{11} = 1, \kappa_1, \kappa_2, \kappa_4) + P(e|d_{11} = 0, \kappa_1, \kappa_2, \kappa_4)\right] \quad (38)$$

where $P(\kappa_1, \kappa_2, \kappa_4)$ is the joint probability distribution of κ_1, κ_2 and κ_4. $P(\kappa_1, \kappa_2, \kappa_4)$ can be calculated as follows

$$P(\kappa_1, \kappa_2, \kappa_4) = P(\kappa_1)P(\kappa_2|\kappa_1)P(\kappa_4|\kappa_1, \kappa_2) \quad (39)$$

From (8), it can be proved that κ_1 and κ_2 are independent. Therefore we have

$$P(\kappa_2|\kappa_1) = P(\kappa_2) \quad (40)$$

Moreover, from (8), κ_1 and κ_2 have binomial distribution as

$$P(\kappa_1) = \frac{\binom{N-1}{\kappa_1}}{2^{N-1}}$$

$$P(\kappa_2) = \frac{\binom{N-1}{\kappa_2}}{2^{N-1}} \quad (41)$$

$P(\kappa_4/\kappa_1, \kappa_2)$ can also be calculated as follows

$$P(\kappa_4|\kappa_1, \kappa_2) = \frac{\binom{\kappa_1}{\kappa_4}\binom{N-1-\kappa_1}{\kappa_2-\kappa_4}}{\binom{N-1}{\kappa_2}} \quad (42)$$

Therefore, from (39)–(42), the joint probability $P(\kappa_1, \kappa_2, \kappa_4)$ can be calculated as

$$P(\kappa_1, \kappa_2, \kappa_4) = \frac{\binom{N-1}{\kappa_1}}{2^{N-1}} \frac{\binom{N-1}{\kappa_2}}{2^{N-1}} \frac{\binom{\kappa_1}{\kappa_4}\binom{N-1-\kappa_1}{\kappa_2-\kappa_4}}{\binom{N-1}{\kappa_2}} \quad (43)$$

Based on the Gaussian assumption of the decision variable, $P(e/d_{11} = 1, \kappa_1, \kappa_2, \kappa_4)$ and $P(e/d_{11} = 0, \kappa_1, \kappa_2, \kappa_4)$ can be calculated as

$$P(e|d_{11} = 1, \kappa_1, \kappa_2, \kappa_4) = Q\left(\frac{\frac{\mathcal{R}wP}{L} - \Delta_{opt}}{\sigma_s(1, \kappa_1, \kappa_2, \kappa_4)}\right)$$

$$P(e|d_{11} = 0, \kappa_1, \kappa_2, \kappa_4) = Q\left(\frac{\Delta_{opt}}{\sigma_s(0, \kappa_1, \kappa_2, \kappa_4)}\right) \quad (44)$$

where $Q(x) = \frac{1}{\sqrt{2\pi}} \int_x^{+\infty} e^{-(u^2/2)}\, du$ and Δ_{opt} is the optimum threshold. Finally, the total error probability is obtained by substituting (43) and (44) in (38). It is noted that the summation in (38) is calculated over the following limits

$$0 \le \kappa_1, \quad \kappa_2 \le N-1$$

$$\max\{\kappa_1 + \kappa_2 - (N-1), 0\} \le \kappa_4 \le \min\{\kappa_1, \kappa_2\} \quad (45)$$

Moreover, the optimum threshold in (44) is chosen such that P_e takes its minimum value.

4 Numerical results

In this section, the BER given in (38) is plotted numerically for the two code sets MQC and Hadamard. The curves are plotted using the following parameters. The receiver load resistance $R_L = 1$ kΩ, $\Delta\nu = 3.5$ THz, $\tau_c = 37.714$ ps, the photodetector responsivity $\mathcal{R} = 1$ and the receiver noise temperature $T^\circ = 300$ K. The optimum threshold, Δ_{opt}, is calculated numerically in the receiver for each N. However, the effect of threshold variation is also investigated in this section. For simplicity, we consider that the pulse $g(t)$ is a rectangular pulse. However, one can obtain the results for other types of pulses. For sake of comparison, we also plot the BER of the synchronous regime obtained in [11].

In the first figure, we investigate the validity of Gaussian approximation of the decision variable. To this end, the

$$I_{2L} = \frac{\lambda}{w-\lambda}\frac{2P\mathcal{R}}{T_b L}\int_0^{T_b} \sum_{m\ge n,(n,i)\ne(m,j)} c_n(i)c_m(j)\bar{c}_1(i)\bar{c}_1(j) \times \Big\{ d_{n1}d_{m1}g(t-\tau_n)g(t-\tau_m)\cos\Big(w_0(\tau_m-\tau_n) + \Delta w((i-j)t + j\tau_m - i\tau_n) + \phi_{ni}(t-\tau_n) - \phi_{mj}(t-\tau_m) + \theta_{ni} - \theta_{mj}\Big) + d_{n1}d_{m2}g(t-\tau'_m)g(t-\tau_n)\cos\Big(w_0(\tau'_m-\tau_n) + \Delta w((i-j)t + j\tau'_m - i\tau_n) + \phi_{ni}(t-\tau_n) - \phi'_{mj}(t-\tau'_m) + \theta_{ni} - \theta'_{mj}\Big) + d_{n2}d_{m1}g(t-\tau'_n)g(t-\tau_m)\cos\Big(w_0(\tau_m-\tau'_n) + \Delta w((i-j)t + j\tau_m - i\tau'_n) + \phi'_{ni}(t-\tau'_n) - \phi_{mj}(t-\tau_m) + \theta'_{ni} - \theta_{mj}\Big) + d_{n2}d_{m2}g(t-\tau'_m)g(t-\tau'_n)\cos\Big(w_0(\tau'_m-\tau'_n) + \Delta w((i-j)t + j\tau'_m - i\tau'_n) + \phi'_{ni}(t-\tau'_n) - \phi'_{mj}(t-\tau'_m) + \theta'_{ni} - \theta'_{mj}\Big)\Big\}\, dt \quad (31)$$

doi: 10.1049/iet-com.2013.0310

normalised histogram of the decision variable, that is, s, for 100 000 different samples is plotted in Fig. 1 together with a Gaussian distribution function when $d_{11} = 0$. In Fig. 1, we neglect thermal and shot noises. The Hadamard codes with length 64 are used, the data rate is 130 Mbps and the number of users is 60. From Fig. 1, it is observed that the normalised histogram of the decision variable is well fitted to the Gaussian distribution function. This shows the validity of using CLT in the analysis.

In addition to Fig. 1, to show the validity of the Gaussian assumption in the analysis, the result of a Kolmogorov–Smirnov (KS) test with 100 000 samples is plotted in Fig. 2. A summary about KS test is presented in the Appendix. In the performed KS test, the parameters same as for Fig. 1 are used. The results are plotted against the number of users. Fig. 2 shows that when the number of users increases then the KS test shows more precise fitness to a Gaussian probability function. This result confirms the Gaussian assumption for the decision variable s.

Fig. 3 shows the BER of the asynchronous SAC-OCDMA in comparison with the synchronous SAC-OCDMA BER obtained in [11] against the number of users for MQC (132, 12, 1) and Hadamard (128, 64, 32) codes. The power of users is set to $P = -10$ dBm and the data rate is 130 Mbps. From Fig. 3, it is observed that the performance of the synchronous regime is degraded more than the asynchronous one. In fact, Fig. 3 shows that the effect of PIIN is more considerable in the synchronous regime. Furthermore, it is observed that the performance of the system with MQC (132, 12, 1) codes is much better than the case with Hadamard (128, 64, 32) codes. This is because in the MQC codes, the cross-correlation between codes is 1 but in the Hadamard codes the cross-correlation is $L/4$.

In Fig. 4, the performance of the system for different data rates is presented. To this end, the BER of the system is plotted against the data rate in Fig. 4. MQC (132, 12, 1) codes are used and the number of users is assumed to be 60 and 80. Moreover, the power of users is −10 dBm. It is observed that if the rate increases then the performance degrades. This is because the variance of the decision variable increases if the rate, that is, $1/T_b$, increases. Note that since in the analysis the assumption $T_b \gg L/\Delta_v$ has been used, the result for very high chip rates, that is, L/T_b, is not plotted in this figure. In fact, for a very high chip rate

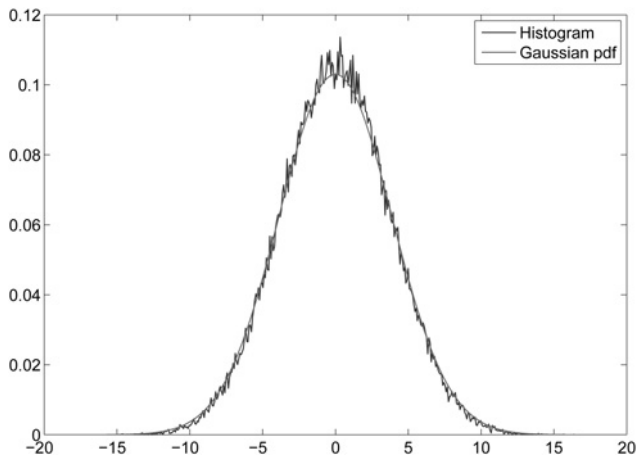

Fig. 1 *Normalised histogram of decision variable compared to a Gaussian distribution function*

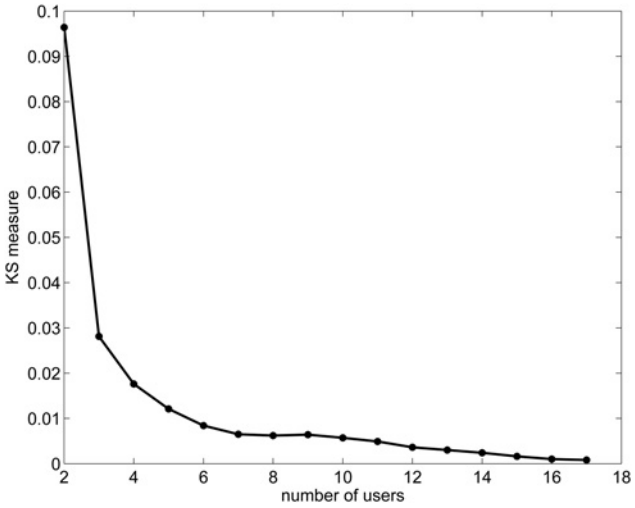

Fig. 2 *KS fitness test results against the number of users*

that the assumption $T_b \gg L/\Delta_v$ is not valid, the result based on the analytic formula in this paper is a lower bound. For the rates used in Fig. 4, it can be shown that the assumption is valid thus the results are exact. However, for very high chip rates that the assumption is not fulfilled a new investigation should be performed to obtain the exact expression of the BER.

In order to show the performance of the system for a very high data rate 1 Gbps, we have to decrease L to fulfill the assumption $T_b \gg L/\Delta_v$. To this end, MQC (56, 8, 1) codes are used. The result is plotted in Fig. 5. It is observed that, for example, for a BER $= 10^{-5}$, 20 users can be supported while from Figs. 3 and 4 for the rates 130 and 500 Mbps, about 120 and 60 users can be supported, respectively.

Fig. 6 shows the BER of the asynchronous SAC-OCDMA using MQC (132, 12, 1) codes for $N = 60$, 80, 120 and the data rate 130 Mbps against the power of each user. It is observed that the effect of PIIN cannot be reduced by increasing the power. Moreover, the performance is degraded for the low power values because of the effect of shot noise and thermal noise.

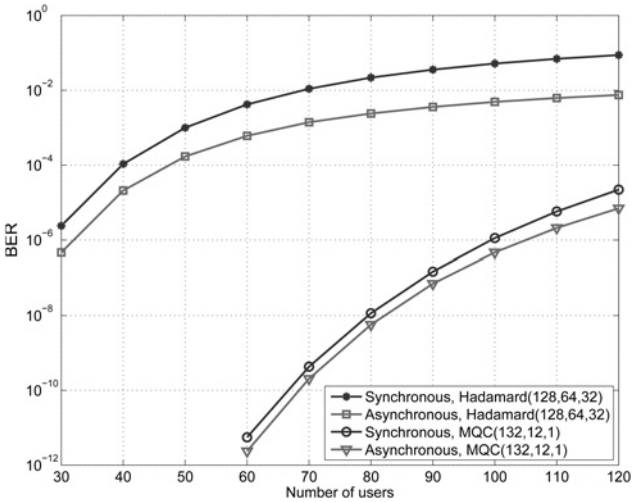

Fig. 3 *BER against the number of users for the synchronous and asynchronous regimes using MQC (132, 12, 1) and Hadamard (128, 64, 32) codes for the rate 130 Mbps*

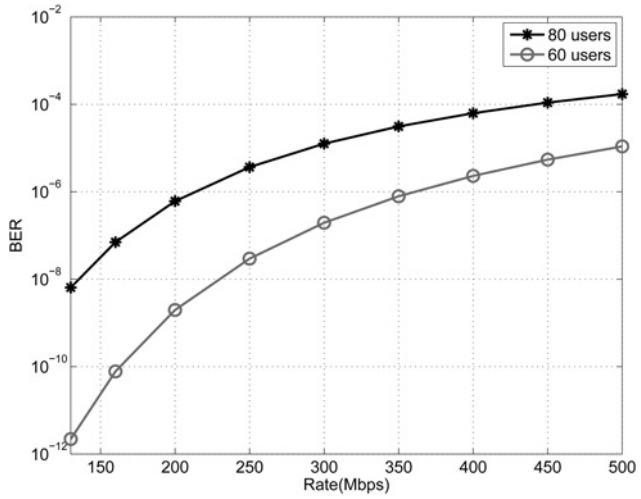

Fig. 4 *BER of the system against the data rate for MQC (132, 12, 1) codes*

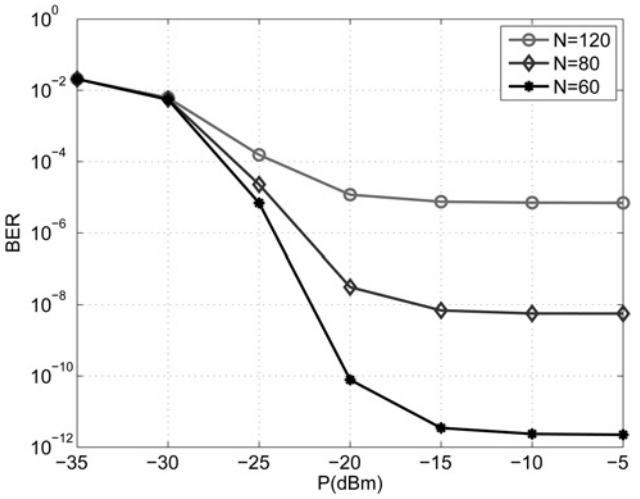

Fig. 6 *Asynchronous SAC-OCDMA BER against the power of each user for MQC (132, 12, 1) codes*

In the previous curves, the threshold is set to the optimum threshold which is a function of the number of active users. However, the number of active users is not known in some cases and it is important to know the impact of threshold variation in the receiver. Fig. 7 shows the effect of variation in the threshold for $N = 80$ and MQC (132, 12, 1). The power of users is set to -10 dBm, the data rate is 130 Mbps. In Fig. 7, the BER is plotted against the normalised threshold, that is, the ratio of threshold to the optimum threshold. Fig. 7 shows the sensitivity of the BER to the variation in the threshold. It is observed that the system is sensitive to the threshold value and choosing a good threshold is an important task in the receiver. It can be also observed that every 10% error in the optimum threshold will result in one order of magnitude error in the BER approximately. This simple state can be helpful for designers of such receivers.

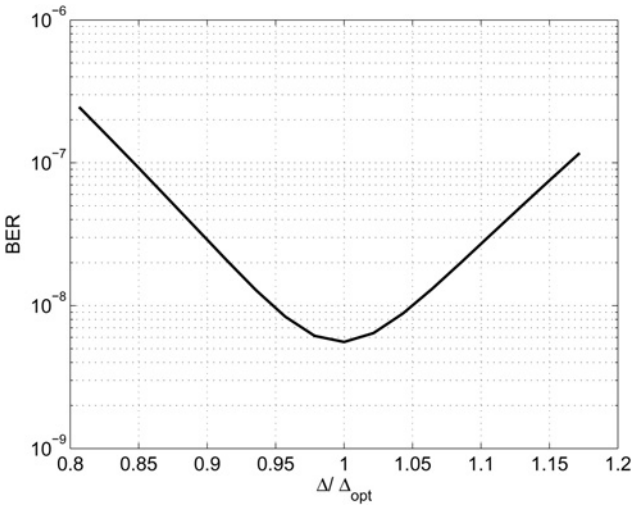

Fig. 7 *Asynchronous SAC-OCDMA BER against the normalised threshold for MQC (132, 12, 1) codes and N = 80*

5 Conclusion and future works

Performance evaluation of a SAC-OCDMA system in the asynchronous regime using the Gaussian approximation for the decision variable was presented. In fact, the mean and the variance of the decision variable in the receiver were obtained considering the effect of the PIIN, shot noise and thermal noise and then the total error probability was obtained. Validity of the Gaussian approximation of the decision variable was also investigated by a KS fitness test. The comparison with the synchronous regime shows a degradation in the synchronous system because of the effect of PIIN, shot noise and thermal noise. In other words, time management in the synchronous regime degrades the performance of a SAC-OCDMA system. Considering the fact that the asynchronous regime is a more attractive candidate for implementation compared to the synchronous one, our analysis gives a realistic picture of the SAC-OCDMA system performance.

In this paper, the BER results for various data rates are presented. However, the analysis is based on the assumption $T_b \gg L/\Delta_v$. This assumption is in fact a limitation on the data rate. For a data rate which does not fulfill this condition, the BER derived in this paper is a lower bound. Therefore an investigation without considering this assumption for very high data rates can be a future work.

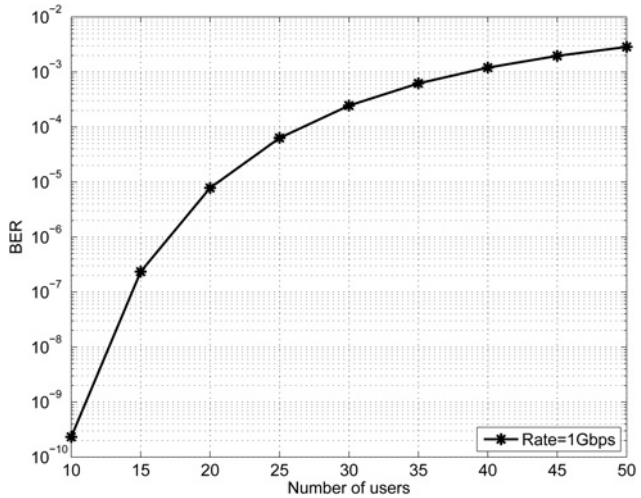

Fig. 5 *BER of the system against the number of users for MQC (56, 8, 1) codes and the rate 1 Gbps*

doi: 10.1049/iet-com.2013.0310

6 References

1 Zaccarin, D., Kavehrad, M.: 'An optical CDMA system based on spectral encoding of LED', *IEEE Photonics Technol. Lett.*, 1993, **4**, (4), pp. 479–482
2 Kavehrad, M., Zaccarin, D.: 'Optical code-division-multiplexed systems based on spectral encoding of noncoherent sources', *J. Lightwave Technol.*, 1995, **13**, (3), pp. 534–545
3 Smith, E.D.J., Blaikie, R.J., Taylor, D.P.: 'Performance enhancement of spectral-amplitude-coding optical CDMA using pulse-position modulation', *IEEE Trans. Commun.*, 1998, **46**, (9), pp. 1176–1185
4 Huang, J.F., Chang, Y.T., Sue, C.C., Hsu, C.C.: 'Hybrid WDM and optical CDMA implemented with M-sequence coded waveguide gratings over fiber-to-the-home network'. IEEE ICC, Circuits and Systems, June 2006, pp. 1860–1864
5 Prucnal, P.R.: 'Optical code division multiple access: fundamentals and applications' (CRC Taylor & Francis Group, 2005)
6 Wei, Z., Ghafouri-Shiraz, H., Shalaby, H.M.H.: 'New code families for fiber-Bragg-grating-based spectral-amplitude-coding optical CDMA systems', *IEEE Photonics Technol. Lett.*, 2001, **13**, (3), pp. 890–892
7 Wei, Z., Ghafouri-Shiraz, H.: 'Proposal of a novel code for spectral amplitude-coding optical CDMA systems', *IEEE Photonics Technol. Lett.*, 2002, **14**, (3), pp. 414–416
8 Zhou, X., Shalaby, H.M.H., Lu, C., Cheng, T.: 'Code for spectral amplitude coding optical CDMA systems', *Electron. Lett.*, 2000, **36**, pp. 728–729
9 Aljunid, S.A., Ismail, M., Ramli, A.R., Ali, B.M., Abdullah, M.K.: 'A new family of optical code sequences for spectral-amplitude-coding optical CDMA systems', *IEEE Photonics Technol. Lett.*, 2004, **16**, (10), pp. 2383–2385
10 Noshad, M., Jamshidi, K.: 'Bounds for the BER of codes with fixed cross correlation in SAC-OCDMA systems', *J. Lightwave Technol.*, 2011, **29**, (13), pp. 1944–1950
11 Shalaby, H.M.H.: 'Closed-form expression for the bit-error rate of spectral-amplitude-coding optical CDMA systems', *IEEE Photonics Technol. Lett.*, 2012, **24**, (15), pp. 1285–1287
12 Ghafouri-Shiraz, H., Karbassian, M.M.: 'Optical CDMA networks: principles, analysis and applications' (John Wiley & Sons, 2012)
13 Rad, M.M., Salehi, J.A.: 'Phase-induced intensity noise in digital incoherent all-optical tapped-delay line systems', *J. Lightwave Technol.*, 2006, **24**, (8), pp. 3059–3072
14 Moslehi, B.: 'Analysis of optical phase noise in fiber optic systems employing a laser source with arbitrary coherence time', *J. Lightwave Technol.*, 1986, **4**, (9), pp. 1334–1351

7 Appendix

KS fitness test is performed as follows

$$\sup_s |F_n(s) - F(s)| \tag{46}$$

where in our case $F(s)$ is the cumulative distribution function (CDF) of a Gaussian random variable and $F_n(s)$ is the estimated CDF of the decision variable using n samples which is calculated as follows

$$F_n(s) = \frac{1}{n}\sum_{i=1}^{n} I_{s_i \le s} \tag{47}$$

In (47), s_i is the ith sample and $I_{s_i \le s}$ is the indicator function, equal to 1 if $s_i \le s$ and equal to zero otherwise.